Structure of Solvated $Fe(CO)_5$: Complex Formation during Solvation in Alcohols

Joshua Lessing,[†] Xiaodi Li, Taewoo Lee,[‡] and Christoph G. Rose-Petruck*

Department of Chemistry, Box H, Brown University, Providence, Rhode Island 02912

Received: July 11, 2007; In Final Form: November 21, 2007

The equilibrium structure of iron pentacarbonyl, $Fe(CO)_5$, solvated in various alcohols has been investigated by Fourier transform infrared (FTIR) measurements and density functional theory calculations. This system was studied because it is prototypical of a larger class of monometallic systems, which are electronically saturated but not sterically crowded. Upon solvation, the $Fe(CO)_5$ is not just surrounded by a solvation shell. Instead, solute−solvent complexes are formed with the oxygen of the alcohol oriented toward an axial ligand of the $Fe(CO)_5$ giving a formation energy on the order of −5 kJ/mol. This complexation is not a chemical reaction but rather a "preassembly" of the solute molecules with a single solvent molecule. For instance, at room temperature the interaction between $Fe(CO)_5$ and ethanol results in 87% of all $Fe(CO)_5$ molecules being complexated with a single ethanol molecule. This complexation was found in all the alcohol systems studied in this paper. The stability of these complexes was found to depend on the alcohol chain length and branching. The observed complexation mechanism is accompanied by an electron density shift from the complexed alcohol molecule toward $Fe(CO)_5$ where it induces a dipole moment. The finding that $Fe(CO)_5$ forms a complex with the hydroxyl group of a single solvent molecule might have significant implications for ligand substitution reactions. This implies that ligand substitution reactions do not have to proceed via a dissociative mechanism. Instead, the reaction might proceed through a concerted mechanism with the leaving CO simultaneously being replaced by the incoming alcohol that was complexed to $Fe(CO)_5$ prior to the photoexcitation.

1. Introduction

Pentacoordinated transition metal carbonyls such as $M(CO)_5$, M = Fe, Ru, and Os, are common place in organometallic syntheses, materials chemistry, and biological processes.[1−6] The dynamics of ligand dissociation and substitution reactions in these systems have been studied extensively in both the gas and liquid phases by static and time-resolved methods.[7−16] Because of the long research history of these compounds, one could think that their structures in solution are well-known. Nevertheless, even the equilibrium solvation structure of iron pentacarbonyl (IPC), and presumably other complexes, is more complicated than generally assumed in the literature. Although theoretically the most stable geometry for $Fe(CO)_5$ and other d^8 systems is trigonal bipyramidal,[17−22] we have shown previously that in aromatic solvent IPC forms stable complexes with one of the solvent molecules thereby distorting the IPC symmetry to C_{2v}.[23,24] For instance, in pentafluorobenzene the IPC−solvent complex has a Gibbs free energy of complexation of −5 kJ/mol, which implies that about 90% of all IPC molecules are complexated with a single solvent molecule. In the resulting complex the solvent molecule is located trans to the apical ligand of $Fe(CO)_5$ ($\sim C_{4v}$). These deformations are possible because pentacoordinated complexes are fluxional and sterically unhindered, enabling ligands to respond to a neighboring solvent molecule by rapidly exchanging their positions.[5,6] In fact, the energy of the D_{3h} structure of IPC is only slightly lower than that for the C_{4v} symmetry. Several d^8 systems that exhibit D_{3h} as well as C_{4v} conformations are known,[25−29] but few studies have investigated[23,24,30−32] the C_{2v} and C_{4v} conformers. During a Berry pseudorotation,[33] the C_{4v} transition state has been calculated to be between 0.6[17,34] and 2.3 kcal/mol[35] above the D_{3h} ground state. Spiess et al.[36] measured a 1 kcal/mol energy barrier for pseudorotation in solution. Therefore, it is clear that in equilibrium a substantial fraction of isolated $Fe(CO)_5$ molecules may be temporarily in C_{4v} configuration.

Here we report on the existence of an IPC−solvent complex in linear and branched alcohols. The complexation energies in these systems are similar to those for arenes, but in alcohols the complexation does not induce a significant structural deformation of IPC. Instead, complexes are formed through the interaction of IPC with the electrons of the alcohol hydroxyl group, which induces a dipole moment in IPC. Our calculations and measurements show that the Gibbs free energy for the IPC−solvent complexation, for instance, in ethanol is about −5 kJ/mol. This implies that the majority of solute molecules are complexed with an alcohol molecule at room temperature. Interestingly, the length and branching of the alcohol chains have a significant influence on the complexation energy. Since the magnitudes of the complexation energies are rather large nearly all solute molecules are complexed. Although we have not carried out time-resolved measurements, we suggest the possibility that $Fe(CO)_5$ ligand substitution reactions do not have to proceed through a dissociative process in alcohols because prior to photoexcitation the incoming alcohol is properly positioned relative to the metal center for ligand binding. Therefore, those IPC molecules that form an IPC−alcohol complex may undergo a concerted ligand substitution reaction upon photodissociation of a carbonyl ligand. Alternatively, IPC molecules which are not complexated should proceed via a dissociative mechanism where the photodissociation of one CO

* Corresponding author. E-mail: Christoph_Rose-Petruck@brown.edu. Phone: (401) 863-1533. Fax: (401) 863-2594.

[†] Current address: Massachusetts Institute of Technology, Cambridge, MA 02139.

[‡] Current address: JILA, University of Colorado, Boulder, CO 80309-0440.

10.1021/jp075421i CCC: $40.75
Published on Web 02/20/2008

ligand is followed by a diffusive encounter of the $Fe(CO)_4$ photoproduct with a single alcohol molecule. Since the relative population of IPC−solvent complexes typically is larger than that of uncomplexed IPC, the concerted reaction mechanism should be dominant. In a noncomplexating solvent, such as cyclohexane, we found that IPC retains its D_{3h} symmetry. Thus, after CO dissociation and vibrational cooling, the triplet ground state of $Fe(CO)_4$ should be reached within picoseconds. This is in agreement with time-resolved infrared spectroscopy experiments carried out by Snee et al.[37] They showed that the UV photolysis of IPC in dry heptane yielded $^3Fe(CO)_4$ exclusively after 26 ps which does not react further for a minimum of 660 ps. This finding in conjunction with earlier results[38] proved that $^3Fe(CO)_4$ has a low level of reactivity in alkanes.

After photolysis the diffusion-controlled reaction should proceed on the picosecond time scale, while the concerted process should proceed on a time scale of ligand dissociation. Gas-phase dissociation studies found that the UV photolysis of IPC causes the loss of a single CO ligand within 150 fs via a conical intersection on the potential energy surface.[14] This photodissociation yields vibrationally hot $^1[Fe(CO)_4]^*$ as the primary product which may loose further ligands within several picoseconds.[14−16] Photolysis of CO ligands from IPC has also been studied using a 620 nm photoexcitation pulse followed by an ultrafast electron diffraction[15] probe. The results show that the major product that forms up to 200 ps after photoexcitation is $^1Fe(CO)_4$, rather than the triplet ground state. They also showed the refined structure of $^1Fe(CO)_4$. The time scale for the ligand substitution in the solution can also be estimated from measurements by Joly and Nelson[12] who used femtosecond transient absorption spectroscopy in the UV spectral range to study the photodissociation of $M(CO)_6$ (M = Cr, Mo, or W) in a variety of linear alcohols. Their data show three distinct time regimes in the photodissociation process: a pulse-duration-limited rise, a rapid nonexponential decay, and a slower exponential rise. The authors associate the first 500 fs with CO ligand dissociation, the 0.5−5 ps interval with solvent complexation, and the 5−50 ps regime with vibrational relaxation of the $M(CO)_5S$ species. They concluded that the solvent complexation dynamics are essentially identical in all solvents. However, the complexation of different solvents causes varying amounts of change in the absorption coefficients. In general agreement with our DFT calculations, Joly and Nelson[12] assume that the complexation through the hydroxyl group is thermodynamically more stable than through the alkyl group. However, this interaction with a solvent molecule occurs after dissociation of the CO ligand from the parent compound. Hexacoordinated complexes are structurally rigid, and therefore, the ligand substitution process has to proceed dissociatively. As the data presented below will show, pentacoordinated complexes can interact with one solvent molecule before photolysis, and we therefore expect that the ligand substitution process in alcohols proceeds at least as fast as several hundred femtoseconds.

Snee et al.[39] reported investigations of the photosubstitution reactions of IPC in methanol, *n*-butyl alcohol, *n*-hexanol, and *t*-butyl alcohol using UV pump transient IR (TIR) absorption probe spectroscopy with a temporal resolution of several picoseconds. They concluded that the photosubstitution of $Fe(CO)_5$ in *t*-butyl alcohol proceed via a $^3Fe(CO)_4$ intermediate. This triplet $^3Fe(CO)_4$ reacts with the hydroxyl group of the entering alcohol, rather than the alkyl group. This is in agreement with the conclusions that we reached from our DFT calculations. We have found that the $Fe-O_{hydroxyl}$ approach is energetically more favorable than the $Fe-C_{methyl}$ approach.

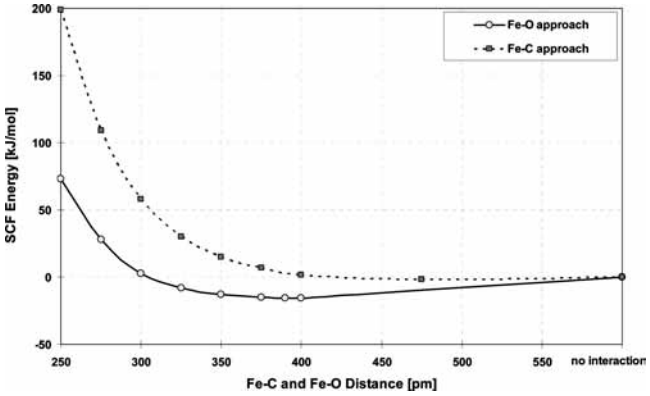

Figure 1. Normalized energy of the IPC−MeOH complex, as a function of constrained distances between iron and the oxygen of MeOH, as well as constrained distances between iron and the carbon atom of MeOH. The figure shows the calculated self-consistent field (SCF) energy. This energy includes the nuclear repulsion, the total one-electron terms (electron−nuclear attraction), and the total two-electron terms (electron−electron repulsion and exchange-correlation).

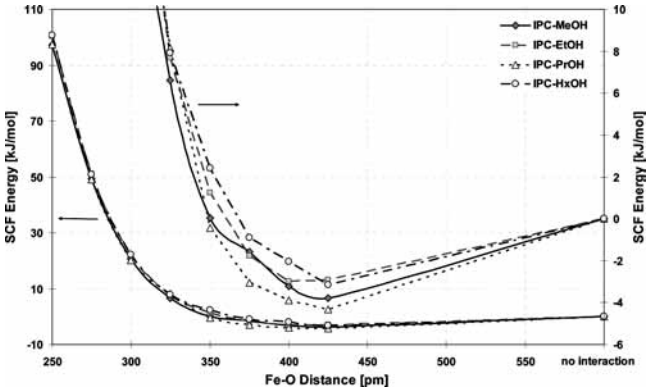

Figure 2. Normalized geometry optimization energy for the IPC−alcohol complex with BSSE correction as a function of the constrained distances between the IPC iron and the alcohol oxygen atom.

Furthermore, Snee et al.[39] concluded that the reactions are diffusion-controlled and depend linearly on viscosity. These conclusions are certainly supported by the authors' data. However, the results of our study, presented here, provide evidence that it is likely that besides the reaction paths documented in the paper of Snee et al., the substitution reaction can also proceed along the reaction path of a concerted ligand substitution process. The latter process should not produce any intermediate $Fe(CO)_4$ and does not proceed through a triplet state. We base this prediction on our evidence that $Fe(CO)_5$ forms a complex with the hydroxyl group of a single solvent molecule before the initiation of the ligand substitution process. Since a diffusive encounter between the $Fe(CO)_4$ and a solvent molecule is not necessary to complete the chemical reaction, the ligand substitution along this reaction pathway does not have to be diffusion-controlled and might proceed through a concerted mechanism where the alcohol binding and CO ligand dissociation occur simultaneously. On the basis of the fact that in equilibrium at room temperature the majority of IPC molecules are complexed with one alcohol molecule, the proposed concerted reaction path could yield a large fraction if not the majority of the reaction products. In fact, although not discussed by Snee et al.,[39] an instantaneous product signature seems to exist at early times for all linear alcohols in Figure 2 of their paper. Such an instantaneous product formation that bypasses any $Fe(CO)_4$ formation is difficult to detect in a TIR experiment

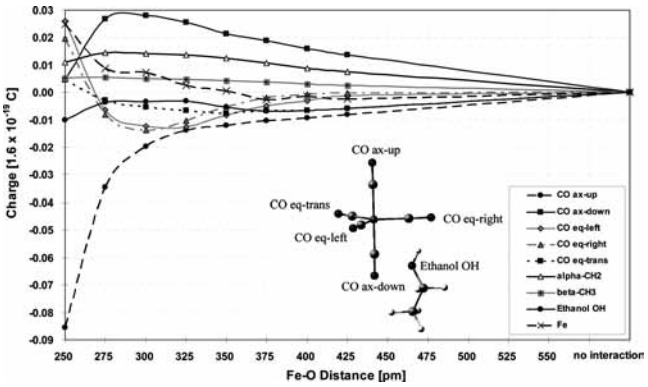

Figure 3. Charge of five CO ligands of IPC and the methyl, hydroxyl group of EtOH at various Fe−O distances.

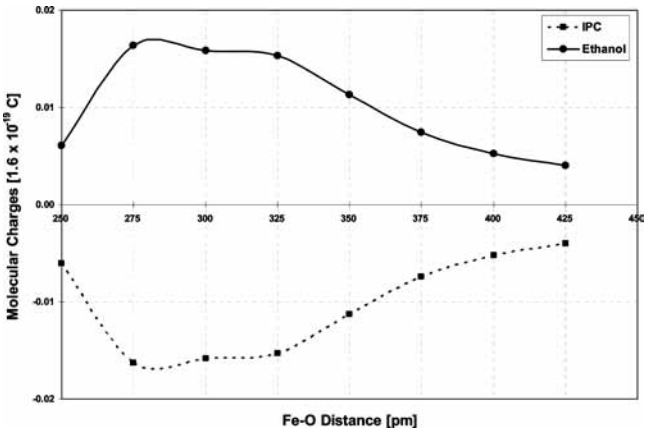

Figure 4. Molecular charges calculated by the NBO method for various constraint Fe−O distances. From this graph, we see the electron transfers from EtOH to $Fe(CO)_5$.

because of the sub-100-fs temporal resolution required and therefore may have been over looked.

In solution one usually finds that excess energy is quickly dissipated into the bath modes of the solvent, and as a result multiple ligand loss typically does not occur.[12,40,41] Nevertheless double substitution after low-intensity UV irradiation has been reported following the one-photon photolysis of IPC with triethylphosphine in isooctane leading to the formation of $Fe(CO)_4(PPh_3)$ and $Fe(CO)_3(PPh_3)_2$ in a ratio of 3:1.[42] In a subsequent study, Nayak and Burkey[43] found that, in the absence of dissolved CO, photolysis of IPC with triethylphosphine in cyclohexane yields $Fe(CO)_3(PEt_3)_2$ with a quantum yield significantly larger than that for $Fe(CO)_4(PEt_3)$. They concluded that double substitution in a single-photon process is possible. However, this does not imply that the substitution process proceeds via the simultaneous dissociation of two CO ligands. Instead, the authors proposed a sequential dissociation mechanism where first a single CO dissociation initially produces $^3[Fe(CO)_4]$ followed by the formation of $^3[Fe(CO)_4(PEt_3)]$. This is followed by a secondary substitution which yields the final product, $Fe(CO)_3(PEt_3)_2$. This explanation differs from the work of Trushin et al.[14] that suggested an S_N2 pathway for the substitution of a CO ligand of $Fe(CO)_4$ with a solvent molecule. In this paper the author disagrees with Nayak et al.'s proposed addition−elimination mechanism because according to Trushin et al. it would necessitate the existence of a $^3Fe(CO)_4L$ intermediate which would be too high in energy to be created. Snee et al.[39] also reported the formation of $Fe(CO)_3(PEt_3)_2$ as well as $Fe(CO)_4(PEt_3)$ from UV-photolyzed IPC in neat triethylphosphine. However, they proposed that after immediate formation of $^3[Fe(CO)_4]$, a $^3[Fe(CO)_3(PEt_3)]$ intermediate was formed via a concerted process in which a second CO ligand is dissociated. The $^3[Fe(CO)_3(PEt_3)]$ intermediate then reacts with another PEt_3 to form the final product, $Fe(CO)_3(PEt_3)_2$.

It is apparent that the chemical dynamics immediately after UV photoexcitation has a significant impact on the products of this photoinitiated reaction. Since the dynamics will depend on IPC's structure before excitation and the compounds interaction with the solvent, the equilibrium structures of solvated IPC were investigated, and the results are presented in this paper.

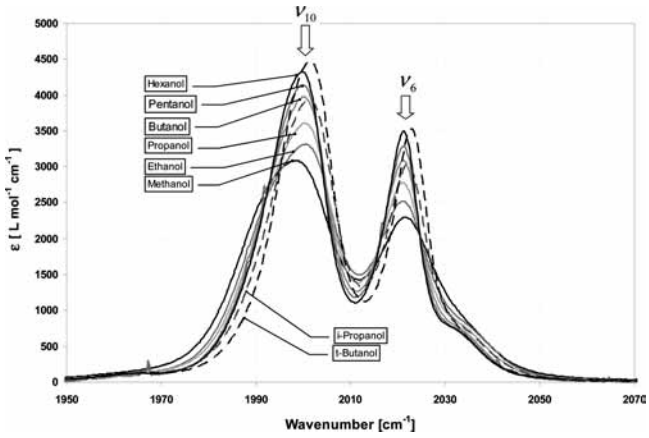

Figure 5. Measured IR absorption spectra of IPC in various alcohols in the spectral range of the strongest absorption peaks. The peak areas are all normalized to the integral absorption coefficient of the ethanol peak. Consequently, the absorbance scale has an uncertainty of ±10%.

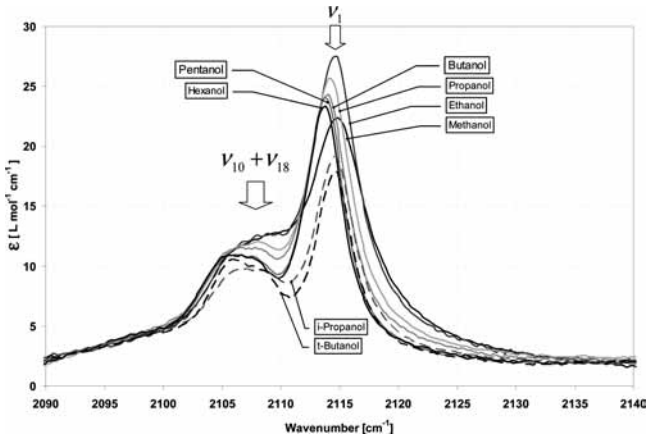

Figure 6. Measured IR absorption spectra of IPC in various alcohols in the spectral range of the ν_1-absorption peak. Baselines were subtracted from each spectrum. The corresponding baselines were obtained from smooth fits to the wings of the separately measured peaks at 2000 cm^{-1}.

TABLE 1: Measured Integrated Absorption Coefficient in the Spectral Range around 2000 cm^{-1} [a]

solvent	integrated absorption coefficient [km/mol]	refractive index
methanol	1081.1	1.328
ethanol	1201.1	1.361
propanol	1232.1	1.385
butanol	1177.5	1.399
pentanol	1167.6	1.410
hexanol	951.8	1.418
isopropyl alcohol	939	1.377
tert-butyl alcohol	1115	1.385

[a] The listed data were corrected for the influences of the solvents' refractive indexes shown in the right column.

TABLE 2: Theoretical Vibrational Frequencies and Absorption Intensities of IR-Active Bands of IPC for Different IPC−EtOH Distances

IPC−solvent structure		M_1[a]		M_2[b]	M_3[c]	M_4[d]	$M_1+M_2+M_3$	$M_4/(M_1+M_2+M_3)$ (%)
C_{4v}	frequency (cm^{-1})	2102.94	2102.94	2110.88	2118.53	2185.7		
	int abs coeff[e]	1320	1320	0	840	4	3480	0.11
250 pm	frequency (cm^{-1})	2079.45	2081.26	2095.79	2112.03	2172.05		
	int abs coeff	878.5	1302.24	703.01	576.91	43.18	3460.66	1.25
275 pm	frequency (cm^{-1})	2081.34	2091.42	2105.02	2122.94	2182.28		
	int abs coeff	1298.96	761.57	751.34	658.68	33.16	3470.55	0.96
300 pm	frequency (cm^{-1})	2085.5	2092.1	2110.96	2126.44	2185.83		
	int abs coeff	1228.67	936.12	579.14	734.26	27.31	3478.19	0.79
325 pm	frequency (cm^{-1})	2087.86	2091.24	2113.09	2126.86	2185.79		
	int abs coeff	1135.69	1065.23	518.88	752.77	21.26	3472.57	0.61
350 pm	frequency (cm^{-1})	2089.45	2092.57	2114.67	2126.96	2186.2		
	int abs coeff	1103.23	1100.05	528.13	745.32	16.67	3476.73	0.48
375 pm	frequency (cm^{-1})	2089.89	2094.48	2115.27	2125.91	2185.96		
	int abs coeff	1115.66	1080.24	597.66	690.88	11.36	3484.44	0.33
400 pm	frequency (cm^{-1})	2090.55	2095.3	2115.81	2125.69	2186.01		
	int abs coeff	1113.93	1082.3	628.5	660.14	10.41	3484.87	0.30
425 pm	frequency (cm^{-1})	2091.45	2095.2	2116.75	2124.6	2186.07		
	int abs coeff	1113.87	1087.58	629.33	658.36	6.79	3489.14	0.19
D_{3h}	frequency (cm^{-1})	2097.47	2124.49	2125.84	2193.1			
	int abs coeff	1119	1118	0	1321	0	3558	0.00

[a] Mode corresponds to $\nu_{10}(D_{3h})$ and $\nu_4(C_{2v}$ and $C_{4v})$. [b] Mode corresponds to $\nu_2(D_{3h})$ and $\nu_3(C_{2v}$ and $C_{4v})$. [c] Mode corresponds to $\nu_6(D_{3h})$ and $\nu_2(C_{2v}$ and $C_{4v})$. [d] Mode corresponds to $\nu_1(D_{3h}, C_{2v}$, and $C_{4v})$. [e] Integrated absorption coefficient [km/mol].

2. Computational Details and Results

The equilibrium populations and structures of IPC−alcohol complexes were calculated and measured based on three methods:

(1) The equilibrium structures and theoretical infrared absorption spectra of the IPC−alcohol complexes were calculated by DFT methods at various distances between IPC and one alcohol molecule. Simultaneously, the calculations provided estimates for the solvent-induced polarization of $Fe(CO)_5$ and the lowest-energy intermolecular distance in the $Fe(CO)_5$–alcohol complex.

(2) Fourier transform infrared (FTIR) spectra of IPC solvated in alcohol solvent were measured, and the spectra were qualitatively analyzed yielding the change of the IPC−alcohol complex populations for various alcohols. The combination of the theoretical and experimental IR absorption spectra additionally permitted estimates for the IPC−alcohol intramolecular distances at equilibrium.

(3) Temperature-dependent FTIR spectra were quantitatively analyzed without any computational input yielding complex populations and the Gibbs free energies of complexation.

2.1. Computational Methods. DFT calculations of the IPC−solvent complex were carried out for methanol, ethanol, propanol, and hexanol using Jaguar.[44] All DFT calculations were performed using the B3LYP model and a LACVP** basis set. Our goal was to calculate the equilibrium structures, vibrational frequencies, IR absorption intensities, and thermodynamic properties of IPC, the alcohol molecules, and the IPC−alcohol complexes at various distances between the iron atom of the IPC and the oxygen atom of the alcohols. The total energy of the IPC−solvent complex was minimized under a fixed iron to alcohol oxygen distance, which was decreased in successive geometry optimizations from 425 to 250 pm. These calculations yielded the complex's energy profile and its equilibrium geometry along this reaction coordinate. At an IPC−solvent distance of 425 pm the solute−solvent interaction was found to be very small, resulting in little deviation from the D_{3h} symmetry. As the distance between iron and the alcohol's oxygen decreased, the electron density distribution of $Fe(CO)_5$ changed from nearly perfect D_{3h} to C_{2v}, which resulted in an induced dipole moment in IPC. This shift was primarily caused by the overlap of the free electron pairs of the alcohol's hydroxyl group with one of the IPC's ligands and, at small approach distances, the iron center. Despite the close approach of the lone pair electrons of the alcohol's hydroxyl group and the induction of a dipole moment in the complex, the IPC possesses only minimal structural deformation. The interaction between IPC and an alcohol molecule through the hydroxyl group is thermodynamically more stable than through the alkyl group. Corresponding computational results of the IPC−methanol complex energies at various intermolecular distances are shown in Figure 1. Although these calculations were not corrected for the basis set superposition error (BSSE), the differences in the energy profile clearly indicate that the complexation through the hydroxyl group is preferred. All subsequent calculations were carried out for this configuration with BSSE correction using the counterpoise method.[45−47]

Figure 2 shows the energy profile for various alcohols. In this figure one notices that a slight minimum of approximately −3 kJ/mol appears at a distance of 400 pm. Within the estimated accuracy of the DFT calculations we consider the minima in all the alcohol systems studied to be identical. Since this is not a Gibbs free energy profile, it only approximately represents the IPC−alcohol complexation in solution. In previous publications[23,48] we calculated the complexation profile as the difference between the Gibbs free energy profile calculated with the IPC in the complex constrained to a D_{3h} symmetry and the Gibbs free energy profile with the IPC being permitted to deform as the solvent molecule, cyclohexane, deuterated benzene, benzene, fluorobenzene, or pentafluorobenzene, approaches. The rational for this procedure was that during the complexation the distance between IPC and the solute molecule should not vary significantly as this would imply a change of solution density. Instead conformational changes are likely occurring at rather constant intermolecular distance. This should also apply here, but significant deformations do not occur at the rather large minimum energy distance. The minimum's position shown in Figure 2 should be a reasonable estimate. It is interesting to note that in these gas-phase calculations an energy minimum

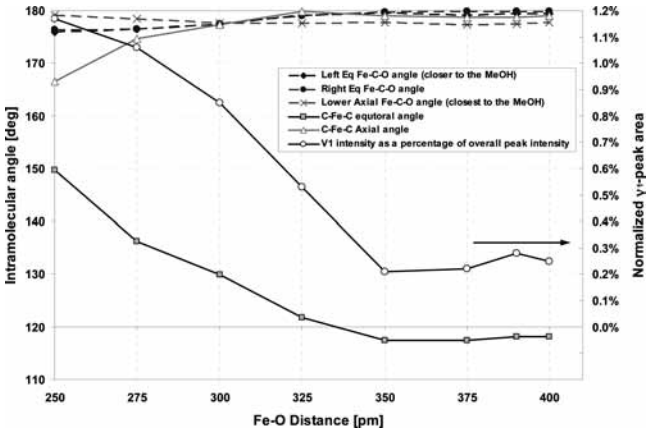

Figure 7. Intramolecular angles and normalized ν_1-peak area calculated for various IPC−methanol distances.

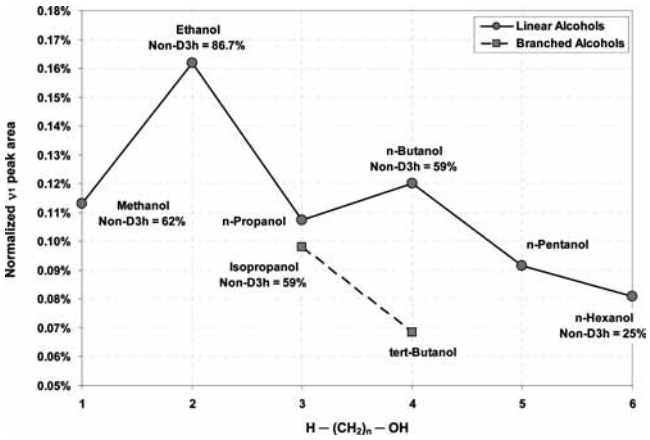

Figure 8. ν_1-Peak areas of $Fe(CO)_5$ measured in various alcohol solvents. The peak areas are normalized to the corresponding areas in the 2000 cm^{-1} range. The absolute complex populations derived from temperature-dependent spectral data are shown as percentages for each solvent system.

for complexation is observed by taking the difference between the D_{3h} constrained and unconstrained trajectories. In the absence of this normalization the IPC−alcohol solvent trajectories show a strictly dissociative energy profile (data not shown). From this observation we can conclude that this complex could not exist in the gas phase, and its observation in solution arises as a result of the congested environment found in condensed phase systems. Nevertheless, the complexation energies and equilibrium distances we report in this publication are primarily based on experimental IR absorption data, and therefore we are convinced that this complex does exist in solution.

2.2. Induction of a Dipole Moment in IPC. The inset in Figure 3 shows that the alcohol molecules approach IPC with the free electron pairs of the hydroxyl oxygen. This suggests that the proximity of the charge from the hydroxyl group to the axial carbonyl ligands pushes electron density toward IPC. Figure 3 shows electron densities for each ligand as a function of distance. The calculations were carried out using the natural bond orbital method (NBO).[49,50] The positive charge of the axial-downward pointing ligand, i.e., of the ligand closest to the alcohol, does increase. Simultaneously, the charge on the axial-upward pointing ligand is reduced. This indicates that the negative charge of the free electrons "pushes" the charges in IPC upward. This effect induces a dipole moment in IPC. Figure 4 shows the overall electronic shift from the alcohol toward IPC. The dipole moment caused by the IPC−alcohol interaction renders normally Raman-active vibrational modes infrared

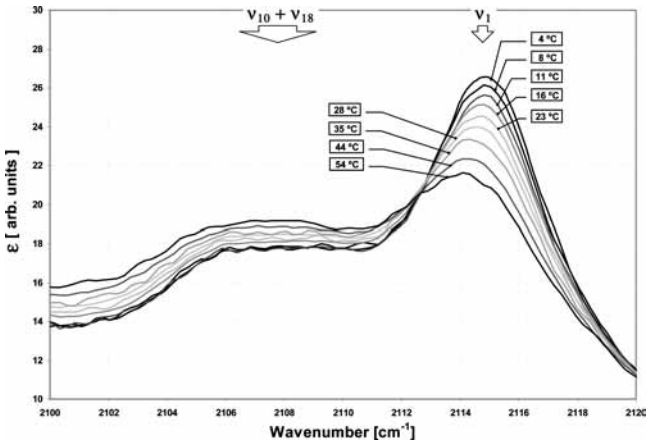

Figure 9. Measured FTIR spectra of 100 mM $Fe(CO)_5$ in ethanol at various temperatures.

active. As a consequence, the intensity of such an infrared-active vibrational mode is a measure of the concentration of IPC−alcohol complexes in solution. A similar method has been applied previously to IPC solvated in arenes.[23,24] However, in those solvents, the infrared appearance of formerly IR-inactive modes was not induced by electronic density shifts but by deformation of IPC from its equilibrium D_{3h} symmetry to a C_{2v} symmetry. In the present study IPC is found to display only a small structural deformation when solvated in the alcohol solvents, and therefore the appearance of new IR-active modes is due primarily to electronic effects.

2.3. Vibrational Frequencies and IR Absorption Intensities. The CO stretching modes of $Fe(CO)_5$ with D_{3h} symmetry are well-known.[51−58] In solution, intense absorption peaks exist between 1967 and 2034 cm^{-1}. These IR peaks are generally red-shifted relative to the gas-phase peaks and, depending on the solvent, are broadened. For a D_{3h} conformer of IPC, these peaks correspond to the IR-active CO stretching modes $\nu_{10}(E')$ and $\nu_6(A_2'')$.[57−65] The E′-mode is doubly degenerate and has a larger intensity than the A_2''-mode. If the D_{3h} symmetry is broken, the degeneracy is lifted and three (overlapping) peaks are observable consisting of four IR-active bands, one of B_1, one of B_2, and two of A_1 symmetries. Owing to their spectral overlap these peaks do not provide much information about the molecular and electronic symmetry of IPC. The ν_1-normal mode at about 2115 cm^{-1} is Raman-active but not IR-active for IPC in D_{3h}. As discussed above, the solvation of IPC in alcohols induces a dipole moment in IPC which, in turn, causes IR absorption of the ν_1-normal mode. The solvent-dependent changes of the absorption peaks are shown in Figures 5 and 6. In general, pentacoordinated metal complexes of the form MA_4B and C_{4v} symmetry have three IR-active bands in the CO stretching region, one of which lies above 2100 cm^{-1}.[32,62,66−69] For IPC in alcohol the ν_1-peak area is a measure of the amount of electron density deformation. Measuring the intensity of the ν_1-mode of solvated IPC in equilibrium provides information about the extent of the electron density deformation as well as the relative population of complexed molecules. The intensity of this absorption line is less than a percent relative to the bands around 2000 cm^{-1}. This might be the reason why the ν_1-line has not been used much in the literature for symmetry evaluations despite the fact that it is very symmetry sensitive and not obscured by other lines.

In addition to the experimental IR data theoretical spectra were calculated for comparison. In these calculations the normal mode frequencies along with their integral IR absorption coefficients were calculated for different IPC−alcohol distances.

TABLE 3: Thermodynamic Parameters from Fits to the Temperature Dependence of the IR Absorption Spectra

						relative populations	
solvent	c	ΔS [J/K mol]	ΔH [kJ/mol]	ΔG at 25 °C [kJ/mol]	K	IPC	complex
methanol	1.3 ± 0.3	-60 ± 22	-19 ± 8	-1.2 ± 1.4	1.6 ± 0.9	$38\% \pm 14\%$	$62\% \pm 14\%$
ethanol	1.02 ± 0.01	-91 ± 7	-32 ± 2	-4.65 ± 0.03	6.53 ± 0.1	$13.3\% \pm 0.1\%$	$86.7\% \pm 0.1\%$
isopropyl alcohol	1.17 ± 0.05	-80 ± 8	-25 ± 3	-0.9 ± 0.2	1.5 ± 0.1	$41\% \pm 2.4\%$	$59\% \pm 2.4\%$
butanol	1.5 ± 0.3	-42 ± 8	-14 ± 3	-0.9 ± 1.0	1.4 ± 0.6	$41\% \pm 10\%$	$59\% \pm 10\%$
hexanol	2 ± 1.4	-105 ± 31	-29 ± 11	3 ± 2.3	0.3 ± 0.3	$75\% \pm 17\%$	$25\% \pm 17\%$

In order to obtain a reasonable approximation of the IPC geometry at various distances, we first energy-minimized the structure of each complex under the constraint of the desired distance between the IPC iron atom and the hydroxyl oxygen atom. For computational reasons, the positions of all IPC atoms were subsequently frozen and the alcohol molecule was removed from the complex. Finally, the single-point energy was recalculated under these constraints. This procedure yielded an IPC geometry that was used to calculate the desired IR parameters. The corresponding integrated absorption coefficients at various IPC−ethanol distances are listed in Table 2. As expected the area of the ν_1-peak increases with decreasing IPC−alcohol distance and therefore can be used as a measure of the IPC−alcohol distance in solution. Figure 7 shows that the increase of the integrated absorption coefficient of the ν_1-peak is not caused by structural deformations. Even at an intramolecular distance of 325 pm, a distance smaller than what we believe to be the equilibrium distance, the axial and equatorial ligand angles correspond to a nearly perfect D_{3h} symmetry, while the absorption coefficient is similar to the measured values.

The sum of the peak areas of the $\nu_6(A_2'')$ and $\nu_{10}(E')$ modes is nearly independent of the IPC−alcohol distance. We therefore used this sum for normalizing all measured ν_1-areas reported below. This normalization additionally removed the influence of the solvents' indexes of refraction.

3. Experimental Details and Results

Infrared absorption spectra were measured with an FTIR spectrometer, model Mattson Infinity Gold FTIR spectrometer. The solvent-dependent changes of the absorption peaks in the spectral range of 2000 cm^{-1} are shown in Figure 5. The peaks were normalized to the integrated absorption coefficient of ethanol. The measured values before normalization are listed in Table 1. All integrated absorption coefficients in Table 1 are corrected for the effects of the refractive indexes of the respective solvents following the discussion given by Polo and Wilson.[70] The normalized values agree with the un-normalized data within ±10%. We believe that the preparation of our solution was accurate to a few percent and therefore conclude that the listed values are accurate as well. This has the consequence that the peak heights do not monotonically increase with alcohol chain length unless they are normalized to a constant peak area. We chose to display the normalized peaks in Figure 5 because it permits the easiest comparison of the peak shapes. The ν_1-vibration mode at 2100 cm^{-1}, shown in Figure 6, is about 200 times less intense. The measured peak areas of the ν_1-mode divided by the un-normalized peak areas in the 2000 cm^{-1} range are displayed in Figure 8 for various alcohols. The peak areas and therefore the equilibrium concentrations of the IPC−alcohol complexes are not a linear function of the alcohol length. It appears that the IPC−ethanol complex has the largest population followed by a steady reduction of the population with increasing alcohol length and branching. This general trend suggests that the IPC−ethanol complex has the most negative Gibbs free energy of complexation of all the alcohols studied.

3.1. Analysis of Temperature-Dependent FTIR Data. The relative peak areas are compared to the IPC−alcohol populations obtained from measurements of the temperature dependence of the ν_1-peak areas. The FTIR spectra at 2100−2200 cm^{-1} for IPC in alcohols were measured at various temperatures in the range from approximately 0−45 °C. A 500 μm thick cell was filled with solutions of approximately 100 mM concentration and mounted in a thermoelectrically controlled sample chamber mounted inside the FTIR spectrometer sample chamber. The temperature distribution within this chamber was uniform and stable a few minutes after selecting the desired temperature. We estimated a ±1 °C uncertainty of the temperature measurements. During the measurements, the FTIR spectrometer sample chamber was flushed with dry nitrogen. Each sequence of temperature-dependent measurements began by taking a room-temperature measurement and was concluded by remeasuring the spectrum at this initial temperature in order to confirm that no chemical modifications had occurred. Measured spectra are shown in Figure 9. The absolute populations can be determined by measuring the normalized ν_1-peak areas at various temperatures because this peak area is proportional to the concentration of IPC−alcohol complexes. The equilibrium constant for the complexation reaction $Fe(CO)_5$ + alcohol ↔ $Fe(CO)_5$···alcohol is the ratio of the concentrations of complexed and uncomplexed IPC. Thus, the Gibbs free energy for the IPC−alcohol complexation can be written as

$$\Delta G_{\text{complex}}(T) = -RT \ln\left(\frac{[\text{complex}]}{[\text{IPC}]}\right) = -RT \ln \left(\frac{[\text{complex}]}{C_{\text{IPC}} - [\text{complex}]}\right) \quad (1)$$

with the initial IPC concentration C_{IPC}. The relative concentration of the complex is then

$$\frac{[\text{complex}]}{C_{\text{IPC}}} = \frac{1}{1 + \text{e}\,\dfrac{\Delta G^{\text{complex}}(T)}{RT}} \quad (2)$$

Since we assume that the ν_1-peak area is proportional to the concentration of complexes, we define a proportionality constant c through

$$\frac{[\text{complex}]}{C_{\text{IPC}}}\, c = \frac{\text{area}_{\nu_1}}{\text{area}_{\nu_6 + \nu_{10}}} \quad (3)$$

We then get

$$\frac{\text{area}_{\nu_1}}{\text{area}_{\nu_6 + \nu_{10}}} = c\, \frac{1}{1 + \text{e}\,\dfrac{\Delta G^{\text{complex}}(T)}{RT}} \quad (4)$$

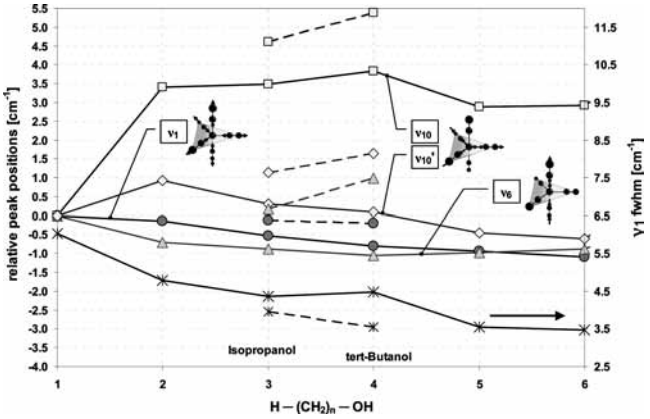

Figure 10. Measured positions of IR absorption peaks of IPC in various alcohols along with the ν_1-peak fwhm of IPC. The insets depict the vibrational modes.

where $\Delta G_{complex}$ is a function of temperature. Assuming, however, that $\Delta H_{complex}$ and $\Delta S_{complex}$ are temperature independent within the temperature range used during our measurements, we write

$$\Delta G_{complex}(T) = \Delta H_{complex} - T\Delta S_{complex} \quad (5)$$

Thus, the functional description of the temperature dependence of the ν_1-peak area contains three temperature-independent fit parameters c, $\Delta H_{complex}$, and $\Delta S_{complex}$. The results of the fitting procedure are listed in Table 3. As expected, the complex population for ethanol is larger than for all other alcohols. For comparison with the relative populations obtained from the normalized ν_1-peak area measurements introduced above in Figure 8, the absolute populations are inserted into the same figure. Both data sets are in general agreement. However, we consider the temperature-dependent data more reliable because all other sample conditions remain unchanged during the experiment and each population number is based on at least 10 measurements.

3.2. Blue-Shift of Peak Centers. The vibrational modes of IPC generally red-shift upon solvation through nonspecific solute−solvent interactions, such as hydrogen bonding. Figure 6 shows that complexation causes a blue-shift with decreasing alcohol chain length. Furthermore, the shifts are temperature dependent, see Figure 9. As the temperature increases, the solution's density decreases and the average IPC−solvent distance increases. Therefore, peak positions caused by nonspecific solvation should blue-shift with increasing temperature and the mode frequencies should approach the gas-phase limits as is the case for low densities. In contrast, we observed blue-shifts upon temperature reduction, which we suggest are caused by the *specific* solvation, i.e., the IPC complex formation. We do not have a well-proven explanation for the blue-shift but we suggest that it is caused by the electron density shifts toward IPC, as shown in Figure 4. As shown in Figure 3, this electron density is unevenly distributed among the five ligands. All equatorial ligands gain electron density. The axial ligand CO_{ax-up} gains electron density but simultaneously $CO_{ax-down}$ loses about twice as much electron density. We speculate that this causes an overall reduction of the electron density in the π-back-bonding orbitals at the axial carbonyl ligands. Since these molecular orbitals are bonding between iron and CO and antibonding between C and O, a reduction of electron density in π-back-bonding orbitals causes a decrease of the iron−ligand strength and a simultaneous increase of the carbonyl bond strengths which, in turn, blue-shifts the CO stretching vibration.

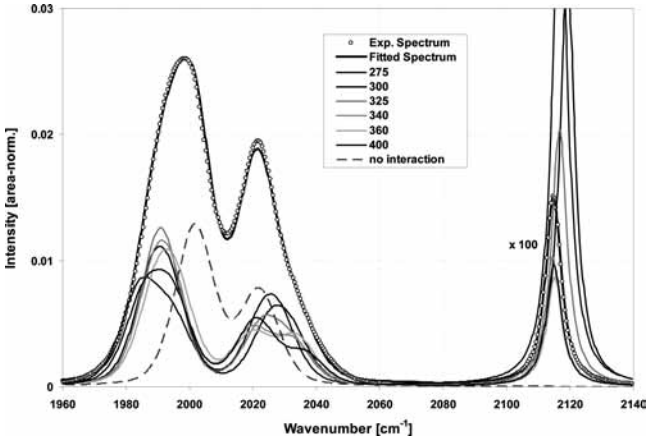

Figure 11. Theoretical IR absorption spectra of IPC in EtOH at various Fe−O distances and the experimental and theoretical fitted FTIR spectra.

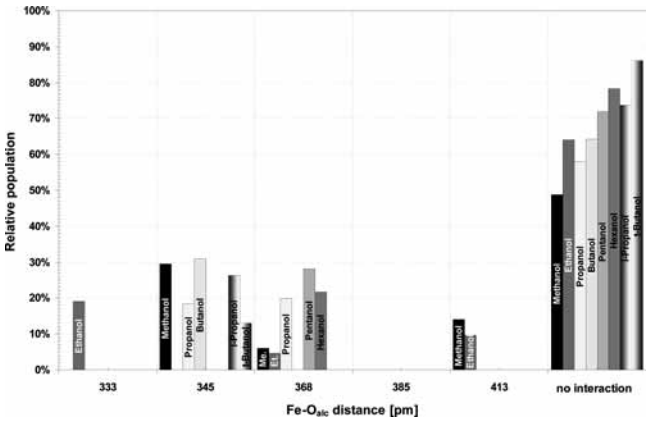

Figure 12. Fitted relative populations of the IPC−solvent distances in various alcohols.

The complexation Gibbs free energy is negative for all solvent systems except hexanol. As the temperature decreases, the complex populations increase and, most likely, the average IPC−alcohol distances decrease. On average the electron density shifts toward IPC increases, and as a result, the measured spectra blue-shift. These results would be consistent with our findings in arenes, which exhibit similar blue-shifts.[23] The idea that the electron density shifts are primarily affecting the π-back-bonding orbitals is also supported by the positions of various normal mode vibrations shown in Figure 10. This figure shows the spectral shifts of the ν_1-, ν_6-, ν_{10}-, and $\nu_{10'}$-peaks along with the width of the ν_1-peak for all alcohols measured. The spectral positions are all normalized to the values for IPC−methanol. The trends of the peaks shifts for higher alcohols are clearly visible. Generally, the blue-shift for the ν_1-peak for smaller alcohols is larger than for larger alcohols. The peak widths increased for smaller alcohols. As shown in the next section, smaller alcohols seem to permit a smaller intramolecular distance. In equilibrium, complexes continuously form and dissociate, and as a consequence small alcohols sample a wider range of intermolecular distances than larger alcohol molecules resulting in a broader distribution of the spectral positions. Since the ν_1-mode is totally symmetric, both equatorial and axial ligands bond strengths influence the frequency. In contrast, the ν_6-mode is a purely axial vibration and follows the trend of the ν_1-peak. The ν_{10}-modes are purely equatorial modes and follow the opposite trend of red-shifting for smaller alcohols. Thus, as the electronic interaction distance becomes smaller, for smaller alcohols, the electron density shift toward the IPC increases. In

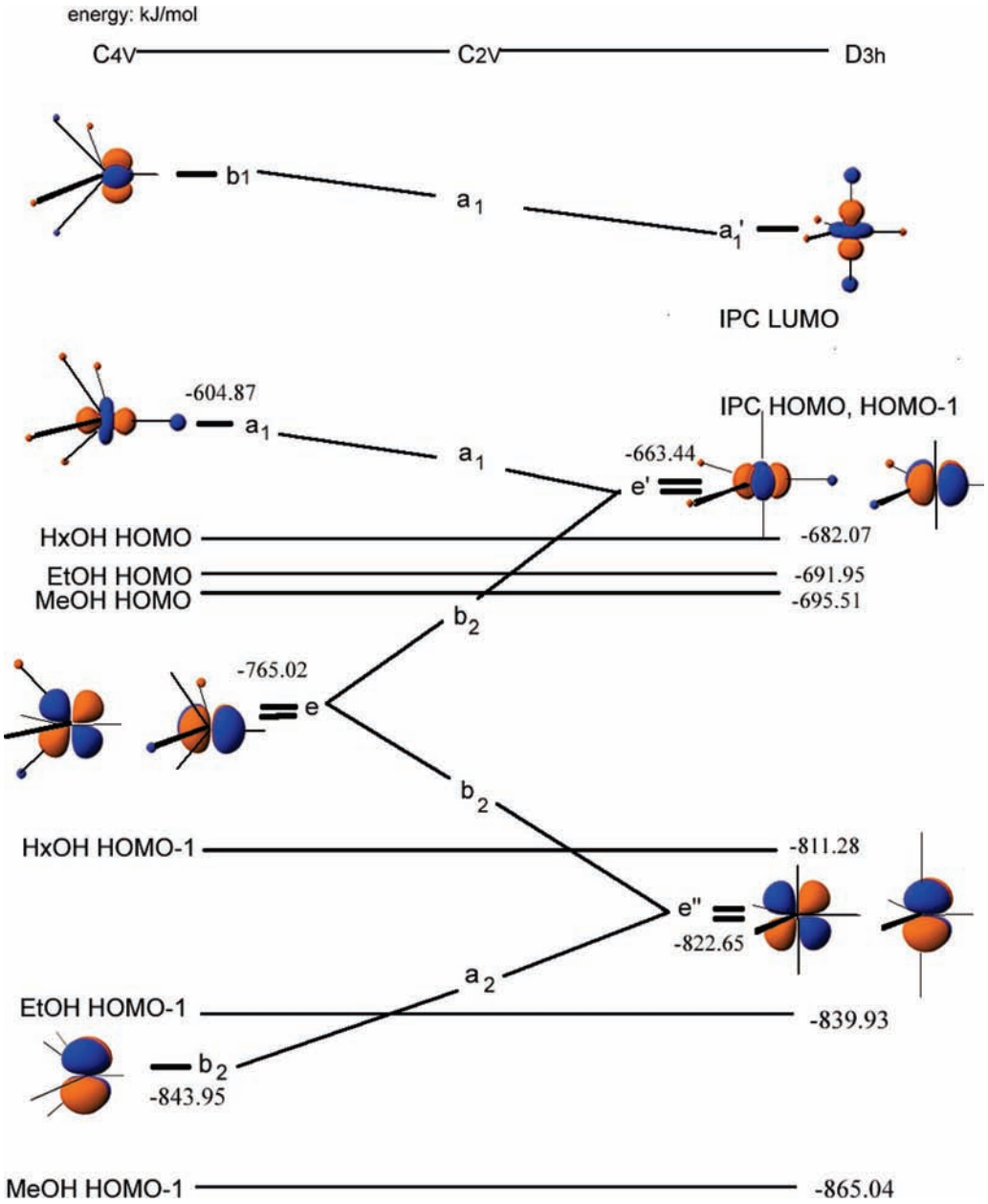

Figure 13. Schematic molecular orbital energy diagram for the IPC and alcohols at various IPC−alcohol distances. For illustration, some simplified molecular orbitals of IPC are shown.

agreement with the concept of π-back-bonding, ligands that on average gain electron density, weaken the C−O bond strength, and the axial ligands that on average lose electron density strengthen their C−O bonds.

3.3. Intermolecular Equilibrium Distances between IPC and Its Complexated Alcohol. The complex population values do not provide any information on the intramolecular distances between IPC and its complexated solvent molecule. The graphs in Figure 2 suggest that the equilibrium $Fe-O_{hydroxyl}$ distances should be in the vicinity of 400 pm. Without structural measurements, accurate values cannot be obtained. However, the equilibrium distances can be estimated from experimental data by fitting the measured FTIR spectra with a superposition of theoretical IR spectra calculated at various $Fe-O_{hydroxyl}$ distances, such as those that were used to compile Table 2. Figure 11 shows the fit of the ethanol spectrum. Prior to fitting with the theoretical spectra, the measured spectrum was first fitted with background curves and curves for the ν_{10}-, ν_6-, and ν_1-modes. In all cases a nearly perfect fit was obtained. Subsequently, the peaks at 2000 cm^{-1} and the ν_1-peak were combined to create the reconstructed experimental spectrum shown as circles. This process yielded a simplified representation of the raw spectrum that contained only peaks that were included in the theoretical description. Furthermore, the intensity of the ν_1-peak was increased by a factor 100 in order to give it a sufficient statistical weight during the fitting process. The theoretical spectra in Figure 11 were obtained through convolution of the calculated mode frequencies with a Lorentzian peak shape with 10 cm^{-1} full width at half-maximum (fwhm). The calculated spectral positions are typically 100 cm^{-1} higher than the experimental values. During the fitting process the positions of the peaks, corresponding to different vibrational modes, were allowed to shift by different offsets relative to the theoretical values. However, these offsets were identical at all intramolecular distances. The fits resulted in nearly identical shifts for all alcohols which lends credence to our fitting procedure.

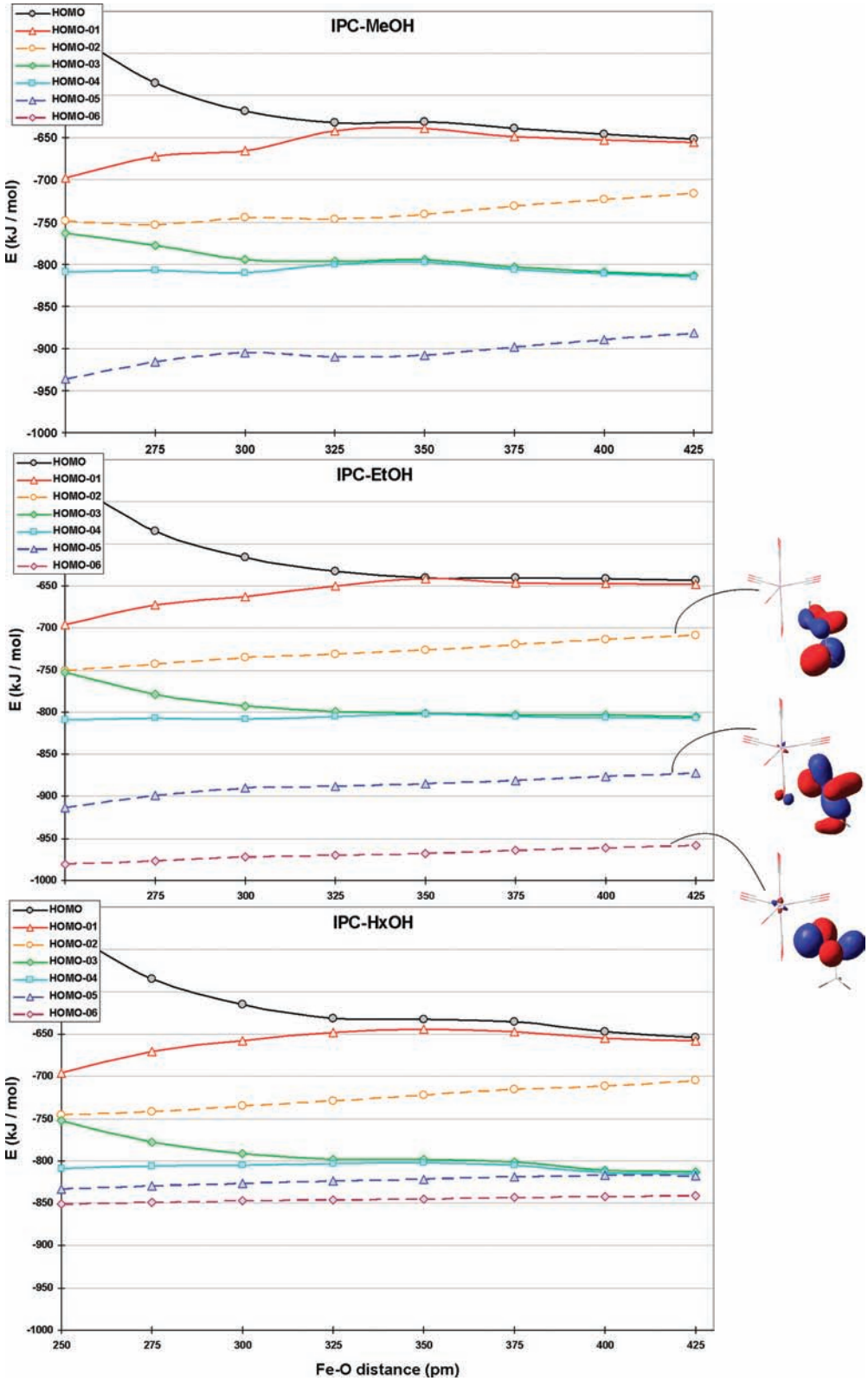

Figure 14. Theoretical molecular orbital energy profiles for various IPC−alcohol complexes. Orbitals primarily derived from alcohol orbitals are plotted as dashed lines, and orbitals primarily derived from IPC orbitals are plotted a solid lines. For instance, the lines HOMO−3 and HOMO−4 correspond to HOMO and HOMO−1 of the isolated alcohols, respectively. Additionally, three DFT-calculated molecular orbitals for the IPC−ethanol complex at 300 pm intramolecular distance are inserted. It can be seen that these orbitals are primarily composed of the HOMO, HOMO−1, and HOMO−2 of the ethanol molecule, respectively.

Specifically, the offsets were approximately -100 cm^{-1} for ν_{10} and ν_6, -80 cm^{-1} for ν_2, and -70 cm^{-1} for ν_1. Figure 12 shows the resulting probability distributions for the intramolecular distances. The most likely distance is approximately 350 pm. It seems that methanol and ethanol tend to approach IPC somewhat closer than the larger alcohols. However, we consider these distributions to be an estimate and not an accurate determination. It is interesting to note that these distances are larger than the intramolecular distances of approximately 260 pm for solvation of IPC in arenes obtained by similar fit

procedures.[23] As a consequence, the complexation with arenes caused a substantial IPC deformation, whereas the complexation with alcohols primarily causes a deformation of the electron density.

3.4. Electronic Structure. The solvation properties presented above can be qualitatively understood through an examination of the changes of the complexes' molecular orbitals with changing intramolecular distance. Figure 13 shows a molecular orbital energy correlation diagram for the deformation of IPC from D_{3h} to C_{4v} symmetry. For illustration, simplified IPC orbitals are depicted next to the corresponding orbitals. Superimposed are the HOMO and HOMO−1 levels of methanol, ethanol, and hexanol. The IPC section of this diagram has been presented before by other authors.[18] The diagram connects the extreme cases of isolated and strongly deformed IPC, for instance, at the transition state of a Berry pseudorotation or during a very close IPC−solvent encounter. As discussed above, a dipole moment is induced in IPC, but the molecule deforms rather little during the complexation. This implies that IPC orbitals indicated on the right (D_{3h}) side of Figure 13 primarily contribute to the molecular orbitals of the complex. It should be noted that even a slight deformation from D_{3h} to C_{2v} increases the energy of the system. The conversion of $Fe(CO)_5$ from D_{3h} to C_{4v} conformation has been calculated to require an energy between 0.6[17,34] and 2.3 kcal/mol.[35] This effect, however, is compensated by the energy changes of the molecular orbitals of the complexes as the intermolecular distance decreases. Figure 14 compares the DFT-calculated molecular orbital energies of the complexes at various intramolecular distances. The energies of the orbitals primarily localized on IPC orbitals are shown as solid lines, and the energies of the orbitals primarily localized on alcohol orbitals are shown as dashed lines. Since the overlap between the orbitals of IPC and the alcohol is rather small, the complex orbitals are nearly identical to the orbitals of the separate molecules. At approximately 350 pm the HOMO, HOMO−1, HOMO−3, and HOMO−4 of all IPC−alcohol complexes have a slight energy maximum which is compensated in smaller alcohol systems by the drop of the energies of alcohol-derived orbitals. This maximum is a consequence of the mixing of IPC and alcohol orbitals. For the highest orbitals, symmetry permits mixing of, for instance, $HOMO-1_{IPC} - HOMO-1_{alcohol} \rightarrow HOMO_{complex}$, $HOMO_{IPC} - HOMO_{alcohol} \rightarrow HOMO-1_{complex}$, and $HOMO_{alcohol} + HOMO_{IPC} \rightarrow HOMO-2_{complex}$. The orbital subtractions and addition explain the formation of the energy maximum for $HOMO_{complex}$ and $HOMO-1_{complex}$ and an energy reduction for $HOMO-2_{complex}$. The other orbitals are mixed in a similar way, but a detailed analysis has not been carried out.

The orbital energies of HOMO−5 and HOMO−6 are higher for large alcohols than for small alcohols. With decreasing intramolecular distance, these energies decrease less the larger the alcohols. This effect might be caused by the larger orbital size of the large alcohols because the overlap integral between IPC and alcohol orbitals will be small and as a result the mixing will have little effect on the orbital energies of the resulting complex. As a consequence, the orbital energies change little as the intermolecular distance decreases. This can be seen in the slight reduction of the energy maximum of HOMO, HOMO−1, HOMO−3, and HOMO−4 at 350 pm with increasing alcohol size. Simultaneously, the slope of HOMO−5 changes from being positive for methanol, to zero for hexanol. The slope of HOMO−6 changes from negative for methanol to positive for ethanol to zero for hexanol. The complex formation energy along the reaction coordinate comprises the energies of all orbitals, as well as the deformation energy of IPC. As a result the largest complex binding energy is found for IPC−ethanol.

4. Conclusion

Our findings show that when IPC is solvated in alcohols the IPC forms weak complexes with a single solvent molecule where no bond is formed between the members of the complex. The complex results from an interaction of the hydroxyl group of an alcohol which shifts electron density from the alcohol to IPC. This deformation of the IPC requires energy which is provided by mixing the orbitals of the IPC and alcohol where the sum of these orbitals determines the overall energy balance for the complex formation. From our gas-phase DFT calculations it was shown that steric factors do not play a significant role in the interaction. Nevertheless the complexation energy is strongly dependent on the alcohol chain length and branching. For example, with a Gibbs free energy of complexation of −4.65 kJ/mol and a 87% population of the complex at room temperature, ethanol forms the strongest complex of all alcohols studied in this paper. In contrast, the interaction between IPC and hexanol is repulsive with a Gibbs free energy of complexation of +3 kJ/mol. This complexation might have significant implications for ligand substitution reactions in solution since the reactant molecules are interacting with each other prior to a reaction. For instance, UV-photoinduced ligand substitution might not proceed via a dissociative process but instead might proceed through a concerted process. In this case the leaving CO would be immediately replaced by an alcohol that was complexed to IPC prior to the photoexcitation (further details for IPC in fluorinated arenes are discussed elsewhere[24]). Since the reactant molecules are interacting with each other prior to the photoexcitation. a diffusive encounter of the reactant molecules may not be required. As a consequence, product formation could be possible before the onset of a full statistical redistribution of energy and, in turn, photoinduced coherent motions could be transferred from IPC to the ligand-substituted product. Realizing the general importance of specific solute−solvent interactions that "preassemble" reactant molecules prior to the induction of a reaction should permit one to choose chemical systems that could proceed faster than bimolecular diffusive-controlled reactions. As a consequence in the case of $Fe(CO)_5$, the formation of reactive intermediates in triplet states should be suppressed and the singlet reaction path should dominate. In principle, such systems could permit the coherent control of the entire bimolecular chemical reaction at room temperature and as a result open new synthetic pathways to desired chemical products.

Acknowledgment. This work was supported by the National Science Foundation (Grant CHE- 0405599). We thank Dr. Christopher M. Laperle for helpful discussions and comments. J.L. and X.L. contributed equally to this work.

References and Notes

(1) Hoye, T. R.; Suriano, J. A. *J. Am. Chem. Soc.* **1993**, *115*, 1154.
(2) Cheng, H.; Reiser, D. B.; Dean, S. W., Jr.; Baumert, K. *J. Phys. Chem. B* **2001**, *105*, 12547.
(3) Knolker, H.-J. *Chem. Soc. Rev.* **1999**, *28*, 151.
(4) Suslick, K. S.; Hyeon, T.; Fang, M.; Cichowlas, A. A. *Adv. Catal. Nanostruct. Mater.* **1996**, 197.
(5) Wrighton, M. *Chem. Rev. (Washington, DC, U.S.)* **1974**, *74*, 401.
(6) Geoffroy, G. L.; Wrighton, M. S. *Organometallic Photochemistry*; Academic Press: New York, 1979.
(7) Bañares, L.; Baumert, T.; Bergt, M.; Kiefer, B.; Gerber, G. *J. Chem. Phys.* **1998**, *108*, 5799.
(8) Heilweil, E. J.; Cavanagh, R. R.; Stephenson, J. C. *J. Chem. Phys.* **1988**, *89*, 230.

(9) Lorono, M.; Cruse, H. A.; Davies, P. B. *J. Mol. Struct.* **2000**, *519*, 199.
(10) Asselin, P.; Soulard, P.; Tarrago, G.; Lacome, N.; Manceron, L. *J. Chem. Phys.* **1996**, *104*, 4427.
(11) Lian, T.; Yang, H.; Asplund, M.; Bromberg, S. E.; Harris, C. B. Femtosecond IR studies of solvation by probing the solvent. In *Springer Series in Chemical Physics*; Toennies, J. P., Ed.; Springer: 1996; Vol. 62, p 300.
(12) Joly, A. G.; Nelson, K. A. *Chem. Phys.* **1991**, *152*, 69.
(13) King, J. C.; Zhang, J. Z.; Schwartz, B. J.; Harris, C. B. *J. Chem. Phys.* **1993**, *99*, 7595.
(14) Trushin, S. A.; Fuss, W.; Kompa, K. L.; Schmid, W. E. *J. Phys. Chem. A* **2000**, *104*, 1997.
(15) Ihee, H.; Cao, J.; Zewail, A. H. *Angew. Chem., Int. Ed.* **2001**, *40*, 1532.
(16) Poliakoff, M.; Turner, J. J. *Angew. Chem., Int. Ed.* **2001**, *40*, 2809.
(17) Demuynck, J.; Strich, A.; Veillard, A. *Nouv. J. Chim.* **1977**, *1*, 217.
(18) Rossi, A. R.; Hoffmann, R. *Inorg. Chem.* **1975**, *14*, 365.
(19) Braga, D.; Grepioni, F.; Orpen, A. G. *Organometallics* **1993**, *12*, 1481.
(20) Beagley, B.; Cruickshank, D. W. J.; Pinder, P. M.; Robiette, A. G.; Sheldrick, G. M. *Acta Crystallogr.* **1969**, *B25*, 737.
(21) Beagley, B.; Schmidling, D. G. *J. Mol. Struct.* **1974**, *22*, 466.
(22) Braga, D.; Grepioni, F.; Orpen, A. G. *Organometallics* **1994**, *13*, 3544.
(23) Jiang, Y.; Lee, T.; Rose-Petruck, C. *J. Phys. Chem. A* **2003**, *107*, 7524.
(24) Lee, T.; Benesch, F.; Jiang, Y.; Rose-Petruck, C. *Chem. Phys.* **2004**, *299*, 233.
(25) Cotton, F. A.; Dunne, T. G.; Wood, J. S. *Inorg. Chem.* **1965**, *4*, 318.
(26) Raymond, K. N.; Corfield, P. W. R.; Ibers, J. A. *Inorg. Chem.* **1968**, *7*, 1362.
(27) Spiro, T. G.; Terzis, A.; Raymond, K. N. *Inorg. Chem.* **1970**, *9*, 2415.
(28) Riedel, E. F.; Jacobson, R. A. *Inorg. Chim. Acta* **1970**, *4*, 407.
(29) Cramer, R. D.; Lindsey, R. V., Jr.; Prewitt, C. T.; Stolberg, U. G. *J. Am. Chem. Soc.* **1965**, *87*, 658.
(30) Apostolova, E. S.; Tikhonov, A. P.; Sendyurev, O. A. *Russ. J. Coord. Chem. (Transl. of Koord. Khim.)* **2002**, *28*, 38.
(31) Tanabe, T.; Morisato, T.; Suzuki, Y.; Matsumoto, Y.; Wadayama, T.; Hatta, A. *Vib. Spectrosc.* **1998**, *18*, 141.
(32) Zaera, F. *Surf. Sci.* **1991**, *255*, 280.
(33) Berry, R. S. *J. Chem. Phys.* **1960**, *32*, 933.
(34) Blyholder, G.; Springs, J. *Inorg. Chem.* **1985**, *24*, 224.
(35) Jang, J. H.; Lee, J. G.; Lee, H.; Xie, Y.; Schaefer, H. F., III. *J. Phys. Chem. A* **1998**, *102*, 5298.
(36) Spiess, H. W.; Grosescu, R.; Haeberlen, U. *Chem. Phys.* **1974**, *6*, 226.
(37) Snee, P. T.; Payne, C. K.; Kotz, K. T.; Yang, H.; Harris, C. B. *J. Am. Chem. Soc.* **2001**, *123*, 2255.
(38) Nayak, S. K.; Burkey, T. J. *J. Am. Chem. Soc.* **1993**, *115*, 6391.
(39) Snee, P. T.; Payne, C. K.; Mebane, S. D.; Kotz, K. T.; Harris, C. B. *J. Am. Chem. Soc.* **2001**, *123*, 6909.
(40) Lian, T.; Bromberg, S. E.; Asplund, M.; Yang, H.; Harris, C. B. *J. Phys. Chem.* **1996**, *100*, 11994.
(41) Joly, A. G.; Nelson, K. A. *J. Phys. Chem.* **1989**, *93*, 2876.
(42) Schroeder, M. A.; Wrighton, M. S. *J. Am. Chem. Soc.* **1976**, *98*, 551.
(43) Nayak, S. K.; Burkey, T. J. *Inorg. Chem.* **1992**, *31*, 1125.
(44) *Jaguar 3.5*; Schrodinger, Inc.: Portland, OR, 1998.
(45) Gutowski, M.; Van Lenthe, J. H.; Verbeek, J.; Van Duijneveldt, F. B.; Chalasinski, G. *Chem. Phys. Lett.* **1986**, *124*, 370.
(46) van Duijneveldt, F. B.; van Duijneveldt-van de Rijdt, J. G. C. M.; van Lenthe, J. H. *Chem. Rev. (Washington, DC, U.S.)* **1994**, *94*, 1873.
(47) Rayon, V. M.; Sordo, J. A. *Theor. Chem. Acc.* **1998**, *99*, 68.
(48) Lee, T.; Welch, E.; Rose-Petruck, C. *J. Phys. Chem. A* **2004**, *108*, 11768.
(49) Reed, A. E.; Weinhold, F.; Curtiss, L. A.; Pochatko, D. J. *J. Chem. Phys.* **1986**, *84*, 5687.
(50) Reed, A. E.; Curtiss, L. A.; Weinhold, F. *Chem. Rev. (Washington, DC, U.S.)* **1988**, *88*, 899.
(51) Jonas, V.; Thiel, W. *J. Chem. Phys.* **1995**, *102*, 8474.
(52) Gutmann, V. *Monatsh. Chem.* **1977**, *108*, 429.
(53) Bor, G. *Inorg. Chim. Acta* **1969**, *3*, 191.
(54) Bor, G. *Inorg. Chim. Acta* **1969**, *3*, 196.
(55) Bor, G.; Jung, G. *Inorg. Chim. Acta* **1969**, *3*, 69.
(56) Bor, G.; Sbrignadello, G.; Marcati, F. *J. Organomet. Chem.* **1972**, *46*, 357.
(57) McClelland, B. W.; Robiette, A. G.; Hedberg, L.; Hedberg, K. *Inorg. Chem.* **2001**, *40*, 1358.
(58) Edgell, W. F.; Dunkle, M. P. *J. Phys. Chem.* **1964**, *68*, 452.
(59) Bigorgne, M. *J. Organomet. Chem.* **1970**, *24*, 211.
(60) Cataliotti, R.; Foffani, A.; Marchetti, L. *Inorg. Chem.* **1971**, *10*, 1594.
(61) Jones, L. H.; McDowell, R. S.; Goldblatt, M.; Swanson, B. I. *J. Chem. Phys.* **1972**, *57*, 2050.
(62) Haas, H.; Sheline, R. K. *J. Chem. Phys.* **1967**, *47*, 2996.
(63) Edgell, W. F.; Wilson, W. E.; Summitt, R. *Spectrochim. Acta* **1963**, *19*, 863.
(64) Swanson, B. I.; Jones, L. H.; Ryan, R. R. *J. Mol. Spectrosc.* **1973**, *45*, 324.
(65) Jones, L. H.; McDowell, R. S. *Spectrochim. Acta* **1964**, *20*, 248.
(66) Adams, D. M. *Metal−Ligand and Related Vibrations: A Critical Survey of the Infrared and Raman Spectra of Metallic and Organometallic Compounds*; Edward Arnold Ltd.: London, 1967.
(67) Cotton, F. A.; Kraihanzel, C. S. *Inorg. Chem.* **1963**, *2*, 533.
(68) El-Sayed, M. A.; Kaesz, H. D. *J. Mol. Spectrosc.* **1962**, *9*, 310.
(69) Farona, M. F.; Cutcliffe, A. B. *Spectrosc. Lett.* **1970**, *3*, 89.
(70) Polo, S. R.; Wilson, M. K. *J. Chem. Phys.* **1955**, *23*, 2376.